

Comparison of Orthogonal Frequency-Division Multiplexing and ON–OFF Keying in Direct-Detection Multimode Fiber Links

Daniel J. F. Barros and Joseph M. Kahn, *Fellow, IEEE*

Abstract—We compare the performance of several direct-detection orthogonal frequency-division multiplexing (OFDM) schemes to that of ON–OFF keying (OOK) in combating modal dispersion in multimode fiber links. We review known OFDM techniques, including dc-clipped OFDM (DC-OFDM), asymmetrically clipped optical OFDM (ACO-OFDM) and pulse-amplitude modulated discrete multitone (PAM-DMT). We describe an iterative procedure to achieve optimal power allocation for DC-OFDM and compare analytically the performance of ACO-OFDM and PAM-DMT. We also consider unipolar M -ary pulse-amplitude modulation (M -PAM) with minimum mean-square error decision-feedback equalization (MMSE-DFE). For each technique, we quantify the optical power required to transmit at a given bit rate in a variety of multimode fibers. For a given symbol rate, we find that unipolar M -PAM with MMSE-DFE has a better power performance than all OFDM formats. Furthermore, we observe that the difference in performance between M -PAM and OFDM increases as the spectral efficiency increases. We also find that at a spectral efficiency of 1 bit/s/Hz, OOK performs better than ACO-OFDM using a symbol rate twice that of OOK. At higher spectral efficiencies, M -PAM performs only slightly better than ACO-OFDM using twice the symbol rate, but requires less electrical bandwidth and can employ analog-to-digital converters at a speed only 81% of that required for ACO-OFDM.

Index Terms—Asymmetrically clipped optical OFDM (ACO-OFDM), communications system performance, intensity modulation with direct detection, minimum mean-square error (MMSE) equalizers, modal dispersion, multicarrier optical systems, multimode fibers, ON–OFF keying (OOK), orthogonal frequency-division multiplexing (OFDM), power allocation, pulse-amplitude modulated discrete multitone (PAM-DMT).

I. INTRODUCTION

RECEIVER-BASED electronic signal processing in optical communication systems has been the subject of many recent studies. Multicarrier modulation has been proposed to combat intersymbol interference (ISI) in multimode fibers since the symbol period of each subcarrier can be made long compared to the delay spread caused by modal dispersion [1]–[3].

The main drawback of multicarrier modulation in systems using intensity modulation (IM) is the high dc bias required to

make the orthogonal frequency-division multiplexing (OFDM) waveform nonnegative. There have been several approaches for reducing the dc power. The first technique uses hard clipping on the negative signal peaks in order to reduce the dc offset required. This method is called dc-clipped OFDM (DC-OFDM). The second technique sets the clipping level at zero, clipping the entire negative excursion of the waveform. Impairment from clipping noise is avoided by appropriate choice of the data subcarrier frequencies [4]. This technique is called asymmetrically clipped optical OFDM (ACO-OFDM). The third technique also clips the entire negative excursion of the waveform, but clipping noise is avoided by modulating only the imaginary components of the subcarriers [5]. This technique is called pulse-amplitude modulated discrete multitone (PAM-DMT).

There have been several studies of the different OFDM techniques (e.g., [6], [7]), but to our knowledge, there has been no comparison of power efficiencies among the various OFDM methods, and to conventional baseband methods, such as ON–OFF keying (OOK). Furthermore, in previous work, the powers of the subcarriers were not optimized for finite bit allocation based on the channel frequency response. We present an iterative procedure for DC-OFDM based on known bit-loading algorithms with a new modification, the bias ratio B_R , in order to obtain the optimum power allocation.

The optimum detection technique for unipolar pulse-amplitude modulation (PAM) in the presence of ISI is maximum-likelihood sequence detection (MLSD), but its computational complexity increases exponentially with the channel memory. ISI in multimode fiber is well approximated as linear in the intensity (instantaneous power) [8], and for typical fibers, PAM with minimum mean-square error decision-feedback equalization (MMSE-DFE) achieves nearly the same performance as MLSD and requires far less computational complexity. Hence, we compare the performance of the three aforementioned OFDM techniques using optimized power allocations to the performance of PAM with MMSE-DFE at different spectral efficiencies.

This paper is organized as follows. In Section II, we review methods for power and bit allocation for multicarrier systems and describe the optimal water-filling solution. We also present the optimal solution for discrete bit allocation, known as the Levin–Campello algorithm [9]. We present our system and fiber models in Section III. In that section, we also discuss the performance measures used to compare different modulations formats. In Section IV, we review the different OFDM formats and study analytically the performance differences between ACO-

Manuscript received May 26, 2010; revised April 08, 2011; accepted May 29, 2011. Date of publication June 09, 2011; date of current version July 22, 2011. This work was supported by the National Science Foundation under Grant ECCS-0700899 and by the Portuguese Foundation for Science and Technology scholarship SFRH/BD/22547/2005.

The authors are with the Department of Electrical Engineering, Stanford University, Stanford, CA 94305-9515 USA (e-mail: djbarros@stanford.edu; jmk@ee.stanford.edu).

Digital Object Identifier 10.1109/JLT.2011.2159192

OFDM and PAM-DMT. In Section V, we compare the receiver electrical SNR required to transmit at a given bit rate for the different OFDM formats and for unipolar PAM with MMSE-DFE equalization at different spectral efficiencies. We present conclusions in Section VI.

II. POWER AND BIT ALLOCATION

A. Gap Approximation

On an additive white Gaussian noise (AWGN) channel, the maximum achievable bit rate is given by the Shannon capacity

$$\frac{C}{B} = \log_2(1 + \text{SNR}) \quad (1)$$

where C is the capacity, B is the channel bandwidth, and SNR is the signal-to-noise ratio. Any real system must transmit at a bit rate less than capacity. For quadratic-amplitude modulation (QAM), the achievable bit rate can be expressed approximately as

$$\frac{R}{B} = \log_2 \left(1 + \frac{\text{SNR}}{\Gamma} \right) \quad (2)$$

where R is the bit rate and Γ is called the gap constant. The gap constant, introduced by Forney and Ungerboeck [10] and Cioffi *et al.* [11], represents a loss with respect to the Shannon capacity. The gap analysis is widely used in the bit loading of OFDM systems, since it separates coding gain from power-allocation gain [12]. For uncoded QAM, the gap constant is given by

$$\Gamma = \frac{\alpha^2}{3} \quad (3)$$

where $\alpha = Q^{-1}(P_e)$, P_e is the symbol-error probability, and Q^{-1} is the inverse Q function. As an example, the gap is 8.8 dB at $P_e = 10^{-6}$ and is 9.5 dB at $P_e = 10^{-7}$ for uncoded QAM. The use of forward error-correction (FEC) codes reduces the gap. A well-coded system may have a gap as low as 0.5 dB at $P_e < 10^{-6}$. A gap of 0 dB means the maximum bit rate has been achieved and therefore $R = C$. Fig. 1 shows the attainable bit rates for various gap values. In the case of real-valued PAM, the gap approximation is valid, but the bit rate is reduced by a factor of two as compared to (2).

For the remainder of this paper, we define the normalized bit rate $b = R/B$, which has units of bit/s/Hz.

B. Optimum Power Allocation

An OFDM signal splits the transmission channel into N parallel channels. When the total average transmitted power is constrained, the maximum obtainable bit rate can be written as

$$\begin{aligned} \max_{P_n} b &= \sum_{n=0}^{N-1} \log_2 \left(1 + \frac{P_n |H_n|^2}{\Gamma \sigma_n^2} \right) \\ \text{subject to } P_t &= \sum_{n=0}^{N-1} P_n \end{aligned} \quad (4)$$

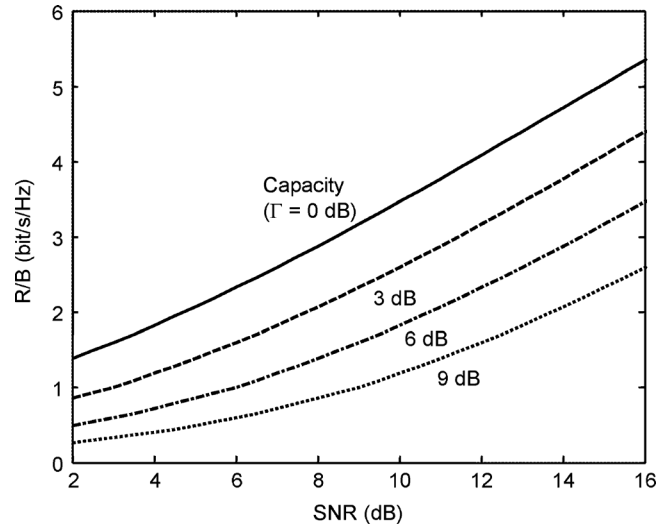


Fig. 1. Achievable bit rate as a function of SNR for various values of the gap Γ .

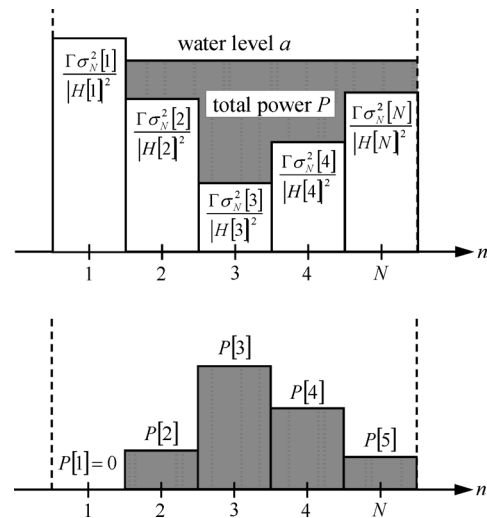


Fig. 2. Optimal power allocation for OFDM.

where $|H_n|^2$, σ_n^2 , and P_n are the channel gain, noise variance, and transmitted power at subcarrier n , respectively, and P_t is the total average transmitted power. The solution of (4) is the known water-filling solution

$$P_n + \frac{\Gamma \sigma_n^2}{|H_n|^2} = a \quad (5)$$

where a is a constant chosen such that $P_t = \sum_n P_n$. The optimum power allocation is then

$$P_n = \begin{cases} a - \frac{\Gamma \sigma_n^2}{|H_n|^2}, & a \geq \frac{\Gamma \sigma_n^2}{|H_n|^2} \\ 0, & a < \frac{\Gamma \sigma_n^2}{|H_n|^2} \end{cases} \quad (6)$$

The optimum power allocation is illustrated in Fig. 2.

After the optimum power allocation is determined, the number of bits to be transmitted on each subcarrier is computed using (2).

We note that when the total average transmitted power is constrained, the optimal power allocation yields a variable data rate. For some applications, a fixed data rate is required. In this case, the optimal design minimizes the average power required to transmit at a given fixed bit rate. The power minimization can be written as

$$\begin{aligned} \min_{P_n} P_t &= \sum_{n=0}^{N-1} P_n \\ \text{subject to } b &= \sum_{n=0}^{N-1} \log_2 \left(1 + \frac{P_n |H_n|^2}{\Gamma \sigma_n^2} \right). \end{aligned} \quad (7)$$

The solution of (7) is also the water-filling solution given by (5). However, in this case, the constant a is chosen such that bit rate is equal to the desired value. We can interpret this solution as the water (power) being poured until the required bit rate is achieved.

C. Optimum Discrete Bit Allocation

While the optimal value of $b = R/B$ is an arbitrary nonnegative real number, in practice, the constellation size and FEC code rate need to be adjusted to obtain a rational number of bits. The optimal discrete bit allocation method is known as the Levin–Campello algorithm [9]. We first choose the desired bit granularity β for each subcarrier, i.e., the bit allocation on each subcarrier will be an integer multiple of β . Next, we choose an initial bit allocation for all the subcarriers (not necessarily optimal). We make the initial bit allocation optimum by using the “efficientizing” (EF) algorithm [9]. Then, depending on the system design, we can either use the “E-tightening” algorithm to obtain the maximum achievable bit rate for a given total power P_t or the “B-tightening” algorithm to obtain the minimum total power required to transmit at a constant bit rate R . We can summarize the Levin–Campello algorithm [9] as follows.

- 1) Choose an initial bit distribution according to β .
- 2) Make the initial bit distribution optimal using the EF algorithm.
- 3) Either use “E-tightening” to obtain the maximum achievable bit rate for a given total power or “B-tightening” to obtain the minimum total power required to transmit at a constant bit rate.

III. OFDM SYSTEM MODEL

A. Overall System Model

The OFDM system model is shown in Fig. 3.

An optical OFDM transmitter encodes transmitted symbols onto an electrical OFDM waveform and modulates this onto the intensity (instantaneous power) of an optical carrier. The modulator can generate one of DC-OFDM, ACO-OFDM, or PAM-DMT. Details of modulators for particular OFDM schemes are described in Section IV.

We assume that there is no optical amplification in the system. After propagating through the multimode fiber, the optical signal intensity is detected, and the electrical current is low-pass filtered. Since we are trying to minimize the optical power required to transmit at given bit rate R , we assume

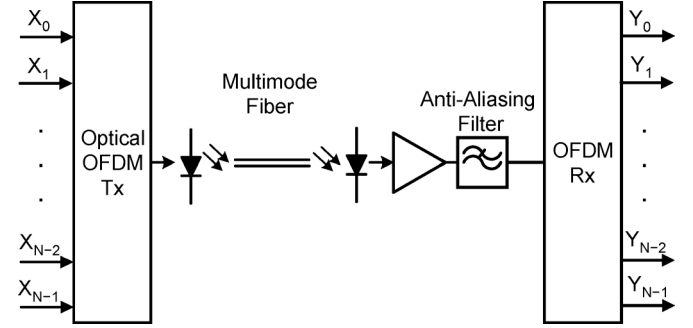


Fig. 3. System model for direct-detection OFDM.

the receiver operates in a regime where signal shot noise is negligible, and the dominant noise is thermal noise arising from the preamplifier following the photodetector. We model the thermal noise as real baseband AWGN with zero mean and double-sided power spectral density $N_0/2$.

After low-pass filtering, the electrical OFDM signal is demodulated and equalized with a single-tap equalizer on each subcarrier to compensate for channel distortion [6], [7].

B. Multimode Fiber Model

There have been several studies on accurately modeling modal dispersion in multimode fibers [13]–[16]. We can express a fiber’s intensity impulse response as [13], [15]

$$h_{\text{MMF}}(t, z) = \left(\sum_n \alpha(n) \delta(t - \tau(n)z) \right) \otimes h_{\text{pulse}}(t) \quad (8)$$

where the set $\alpha(n)$ is known as the mode power distribution, $\tau(n)$ is the group delay per unit length of the n th principal mode, and $h_{\text{pulse}}(t)$ is the pulse shape of a principal-mode group. The parameters $\alpha(n)$ and $\tau(n)$ depend not only on the fiber index profile but also on the fiber input coupling, the input excitation, connectors offsets, and fibers bends. Hence, these parameters are usually modeled as random variables.

The group delay parameter $\tau(n)$ is characterized by the differential-mode delay (DMD), which is the difference between the fastest and slowest principal-mode groups. In our model, we choose $\tau(n)$ as an exponential random variable, $\alpha(n)$ as a Gaussian power profile, and $h_{\text{pulse}}(t)$ as a second-order super-Gaussian pulse. We choose the full-width at half-maximum of the pulse shape of a principal-mode group [$h_{\text{pulse}}(t)$] to vary inversely with the mean group delay ($E[\tau(n)]$) such that the fiber 3-dB bandwidth would scale inversely proportional to the fiber length, as presented in [15]. We adjust the parameters such that our set of fibers is very similar to the fibers in [13] and [14] at a wavelength of 850 nm. Specifically, we have created 1728 fibers with DMDs between 0.2 and 0.7 ns/km and with 19 principal-mode groups propagating.

Fig. 4 shows the mode power distribution, mode delays, and frequency response for an exemplary fiber from our set. In our study, we choose a fiber length of 1 km.

Fig. 5 shows the 3-dB bandwidth distribution of all the fibers used in our analysis.

As we can observe, the 3-dB bandwidths obtained are consistent with the range of values encountered in [13], [16].

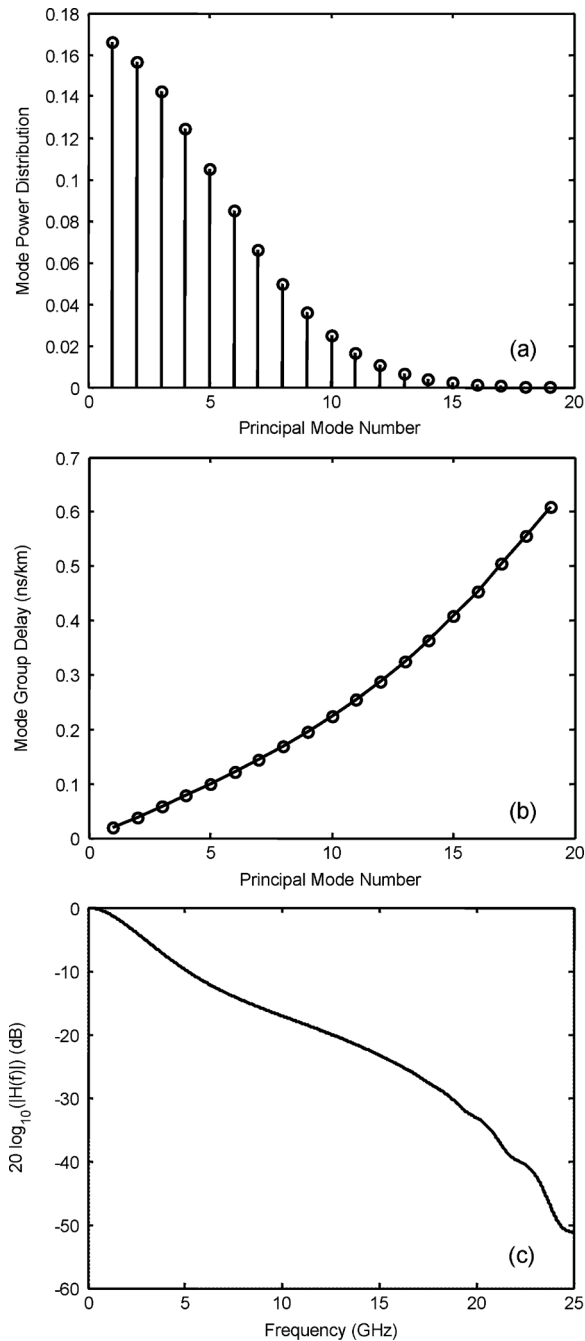


Fig. 4. (a) Mode power distribution, (b) mode delays, and (c) frequency response for fiber 1183. We consider a 1-km length in computing the delays and frequency response.

C. Performance Measures

Our baseband channel model is given by

$$y(t) = R \cdot x(t) \otimes h_{\text{MMF}}(t) + n(t) \quad (9)$$

where $y(t)$ is the electrical detected signal, $x(t)$ is the input intensity waveform, $h_{\text{MMF}}(t)$ is the fiber intensity impulse response, $n(t)$ is the thermal noise from the photodetector preamplifier, and R is the photodetector responsivity (A/W). This model differs from conventional electrical systems because the channel input represents instantaneous optical power (i.e.,

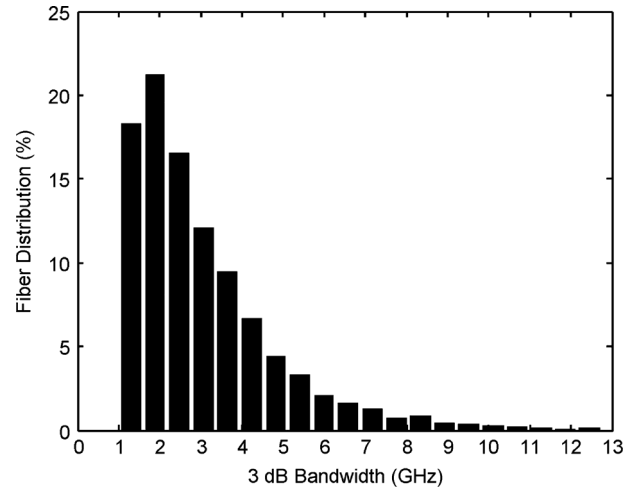


Fig. 5. 3-dB bandwidth distribution of the multimode fibers simulated. All fibers have 1-km length.

intensity). Hence, the channel input is nonnegative ($x(t) \geq 0$) and the average transmitted optical power P_t is given by

$$P_t = \lim_{T \rightarrow \infty} \frac{1}{2T} \int_{-T}^T x(t) dt \quad (10)$$

rather than the usual time average of $|x(t)|^2$, which is appropriate when $x(t)$ represents amplitude. The average received optical power can be written as

$$P = H_{\text{MMF}}(0) P_t \quad (11)$$

where $H_{\text{MMF}}(0)$ is the dc gain of the channel, i.e., $H_{\text{MMF}}(0) = \int_{-\infty}^{\infty} h_{\text{MMF}}(t) dt$.

In order to facilitate comparison of the average optical power requirements of different modulations techniques at a fixed bit rate, we define electrical SNR as [17]

$$\text{SNR} = \frac{R^2 P^2}{N_0 R_b} = \frac{R^2 H_{\text{MMF}}^2(0) P_t^2}{N_0 R_b} \quad (12)$$

where R_b is the bit rate and N_0 is the (single-sided) noise power spectral density. We see that the SNR given by (12) is proportional to the square of the received optical signal power P , in contrast to conventional electrical systems, where it is proportional to the received electrical signal power.

A useful measure of the ISI introduced by a multimode fiber is the temporal dispersion of the impulse response expressed by the channel root-mean-square (rms) delay spread D [18]. The rms delay spread D can be calculated as [18]

$$D = \left[\frac{\int (t - \mu)^2 h_{\text{MMF}}^2(t) dt}{\int h_{\text{MMF}}^2(t) dt} \right]^{1/2} \quad (13)$$

where the mean delay μ is given by

$$\mu = \frac{\int t \cdot h_{\text{MMF}}^2(t) dt}{\int h_{\text{MMF}}^2(t) dt} \quad (14)$$

Fig. 6 shows the channel rms delay spread D distribution of all the fibers used in our analysis.

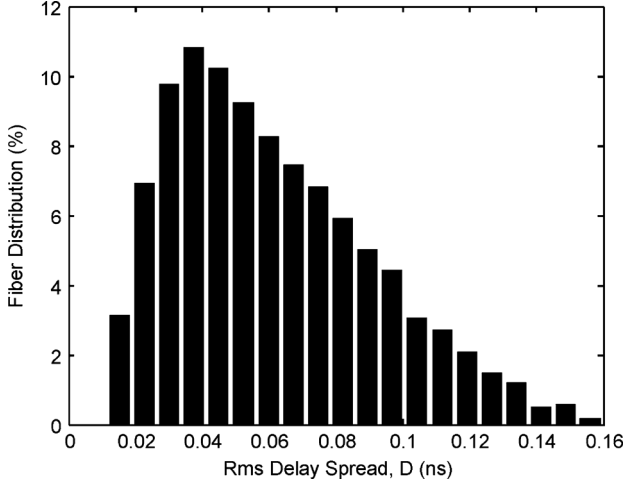


Fig. 6. RMS delay spread D distribution of the multimode fibers simulated. All fibers have 1-km length.

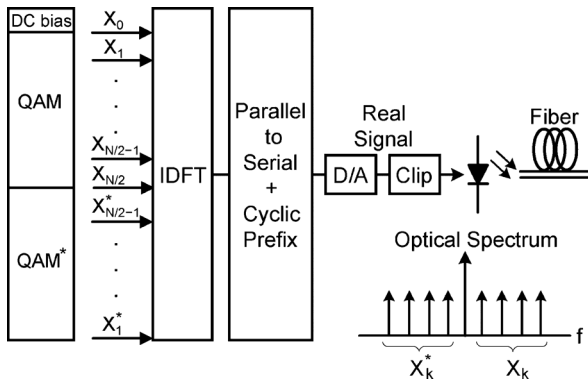


Fig. 7. Block diagram of a DC-OFDM transmitter.

We will also use the normalized delay spread D_T , which is a dimensionless parameter defined as the rms delay spread D divided by the bit period T_b ($T_b = 1/R_b$):

$$D_T = \frac{D}{T_b}. \quad (15)$$

IV. ANALYSIS OF DIRECT-DETECTION OFDM SCHEMES

A. DC-OFDM

The main disadvantage of using OFDM with IM is the dc bias required to make the OFDM signal nonnegative. Since OFDM signals have a high peak-to-average ratio, the required dc bias can be high. A simple approach to reduce the dc offset is to perform hard clipping on the negative signal peaks [4]. This technique is usually called DC-OFDM. A DC-OFDM transmitter is shown in Fig. 7.

In Fig. 7, the transmitted symbols are modulated such that the time-domain waveform is real. This is achieved by enforcing Hermitian symmetry in the symbols input to the inverse discrete Fourier transform. We note that the zero (dc) subcarrier is not modulated and is equal to the dc offset. After digital-to-analog (D/A) conversion, the electrical OFDM signal is hard clipped such that the waveform becomes nonnegative, and then the signal is intensity modulated onto the optical carrier.

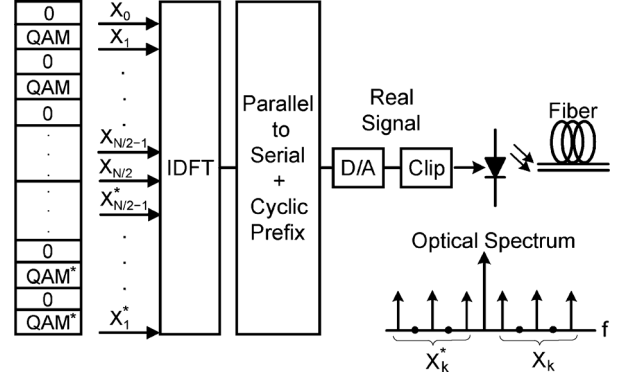


Fig. 8. Block diagram of an ACO-OFDM transmitter.

For a high number of subcarriers, we can model the electrical OFDM signal $x(t)$ as a Gaussian random variable with mean equal to the dc bias and variance equal to the electrical power $\sigma^2 = E[|x(t)|^2]$. After hard clipping at zero, we obtain only the positive side of the Gaussian distribution. We can show that the average of the clipped DC-OFDM signal is given by

$$P_{\text{DC-OFDM}} = E[x_{\text{clip}}(t)] = \frac{\sigma}{\sqrt{2\pi}} e^{-\frac{\gamma^2}{2\sigma^2}} + \gamma \left(1 - Q\left(\frac{\gamma}{\sigma}\right)\right) \quad (16)$$

where Q is the Q function and γ is the dc bias. If we choose the dc bias to be proportional to the square root of the electrical power, i.e., $\gamma = B_R \cdot \sigma$ where B_R is the proportionality constant, then minimizing the electrical power also minimizes the optical power required. We note that if the dc bias is chosen such that there is no clipping, then the optical power is equal to the dc bias γ , as expected.

B. ACO-OFDM

Armstrong *et al.* showed that in an OFDM system, clipping noise is avoided by encoding information symbols on only the odd subcarriers [4]. This technique is called ACO-OFDM. Fig. 8 shows a block diagram of an ACO-OFDM transmitter.

As in DC-OFDM, the OFDM subcarriers are assumed to have Hermitian symmetry, so that the time-domain waveform is real. Because only the odd subcarriers are used to transmit data, for a given choice of signal constellation, ACO-OFDM has only half the spectral efficiency of DC-OFDM. After D/A conversion, the electrical OFDM signal is hard clipped at zero and intensity modulated onto an optical carrier.

For a high number of subcarriers, we can model again the electrical OFDM signal $x(t)$ as a Gaussian random variable but for ACO-OFDM the electrical signal has a zero mean. After hard clipping at zero, we obtain again only the positive side of the Gaussian distribution. We can show that the average of the clipped Gaussian is $\sigma/\sqrt{2\pi}$ and that the variance is $\sigma^2/2$. Hence, the average optical transmitted power in ACO-OFDM is

$$P_{\text{ACO-OFDM}} = \frac{\sigma}{\sqrt{2\pi}}. \quad (17)$$

As we can observe in (17), the average optical power is proportional to the square root of the electrical power.

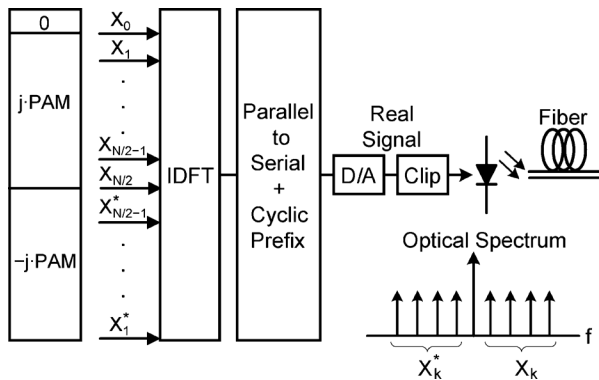


Fig. 9. Block diagram of a PAM-OFDM transmitter.

C. PAM-DMT

A similar approach for reducing the required dc bias is to use PAM-DMT. Lee *et al.* [5] showed that the clipping noise becomes orthogonal to the desired signal if only the imaginary parts of the subcarriers are modulated. If PAM modulation is used on the imaginary components of the subcarriers, the clipping noise does not affect the system performance since that noise is real valued, i.e., orthogonal to the modulation. Fig. 9 shows a block diagram of a PAM-DMT transmitter.

As in DC-OFDM and ACO-OFDM, the OFDM subcarriers for PAM-DMT are assumed to have Hermitian symmetry, so that the time-domain waveform is real. Contrary to ACO-OFDM, in PAM-DMT all of the subcarriers are used, but the modulation is restricted to just one dimension. Hence, PAM-DMT has the same spectral efficiency as ACO-OFDM. After D/A conversion, the electrical OFDM signal is hard clipped at zero and intensity modulated onto an optical carrier.

Using the same analysis as for ACO-OFDM, one can show that the average transmitted optical power for PAM-DMT is also given by

$$P_{\text{PAM-DMT}} = \frac{\sigma}{\sqrt{2\pi}} \quad (18)$$

where σ is the square root of the electrical power of the unclipped OFDM waveform.

It is useful to compare the performance of PAM-DMT and ACO-OFDM. We first compare the performance in the limit of a small number of subcarriers. The minimum number of subcarriers is five, such that two are used for data, the other two are Hermitian conjugates of the data subcarriers, and the fifth is the dc subcarrier, which is set to zero. For ACO-OFDM, only one of the two possible subcarriers is used for data transmission. Thus, for a given total power P_t , the normalized bit rate is given by

$$b_{\text{ACO}} = \log_2 \left(1 + \frac{P_t |H_1|^2}{\Gamma \sigma^2} \right) \quad (19)$$

where H_1 is the channel gain at the first subcarrier.

In PAM-DMT, all the subcarriers are used for data transmission but the modulation is restricted to one dimension, i.e.,

PAM. The optimum power allocation for PAM-DMT is given by (5) and can be written as

$$P_n + \frac{\Gamma (\sigma_n^2/2)}{|H_n|^2} = a. \quad (20)$$

We note that the noise variance in (20) is half than in ACO-OFDM because in PAM-DMT, only one dimension is being modulated. The constant a can be found by using (6) and $P_t = P_1 + P_2$. The optimum power allocation for the two subcarriers is then

$$\begin{aligned} P_1^{\text{opt}} &= \frac{P_t}{2} + \delta \\ P_2^{\text{opt}} &= \frac{P_t}{2} - \delta \end{aligned} \quad (21)$$

where δ is given by

$$\delta = \frac{1}{4} \sigma^2 \Gamma \left(\frac{1}{|H_2|^2} - \frac{1}{|H_1|^2} \right). \quad (22)$$

The maximum normalized bit rate for PAM-DMT is

$$\begin{aligned} b_{\text{PAM}} &= \frac{1}{2} \log_2 \left(1 + \frac{P_1^{\text{opt}} |H_1|^2}{\Gamma \sigma^2/2} \right) \\ &\quad + \frac{1}{2} \log_2 \left(1 + \frac{P_2^{\text{opt}} |H_2|^2}{\Gamma \sigma^2/2} \right) \\ &= \log_2 \left(\sqrt{1 + \frac{(P_t/2 + \delta) |H_1|^2}{\Gamma \sigma^2/2}} \right) \\ &\quad \cdot \sqrt{1 + \frac{(P_t/2 - \delta) |H_2|^2}{\Gamma \sigma^2/2}} \end{aligned} \quad (23)$$

We now assume that the channel has a low-pass frequency response, such that $|H_2| < |H_1|$. This assumption is valid for the majority of multimode fibers. We obtain an upper bound on (23) as

$$\begin{aligned} b_{\text{PAM}} &\leq \log_2 \left(\sqrt{1 + \frac{(P_t/2 + \delta) |H_1|^2}{\Gamma \sigma^2/2}} \right) \\ &\quad \cdot \sqrt{1 + \frac{(P_t/2 - \delta) |H_1|^2}{\Gamma \sigma^2/2}} \\ &\leq \log_2 \left(\sqrt{\left(1 + \frac{(P_t/2) |H_1|^2}{\Gamma \sigma^2/2} \right)^2 - \left(\frac{\delta |H_1|^2}{\Gamma \sigma^2/2} \right)^2} \right) \\ &< \log_2 \left(1 + \frac{P_t |H_1|^2}{\Gamma \sigma^2} \right) \\ &< b_{\text{ACO}}. \end{aligned} \quad (24)$$

From (24), we observe that ACO-OFDM is more power efficient than PAM-DMT for a small number of subcarriers on low-pass channels. Furthermore, from (24), we see that if the channel is flat, i.e., $|H_1| = |H_2|$, then $\delta = 0$ and both techniques have exactly the same power efficiency.

For a high number of subcarriers, we can apply a similar analysis for each pair of used subcarriers. Since $|H_{n+1}| \approx |H_n|$ for a high number of subcarriers, the power efficiency of PAM-DMT converges asymptotically to that of ACO-OFDM for low-pass channels in the limit of a high number of subcarriers.

V. COMPARISON OF DIRECT-DETECTION MODULATION FORMATS

The system model is shown in Fig. 3. As mentioned previously, we neglect all transmission impairments except for modal dispersion of the multimode fiber. We employ the fiber model discussed in Section III-B, assuming a fiber length of 1 km and transmission at 850 nm.

We assume the dominant noise is thermal noise, modeled as real baseband AWGN with zero mean and double-sided power spectral density $N_0/2$. We choose $N_0 = 10^{-22}$ A²/Hz, which is a typical value for commercial optical receivers. We assume a photodetector quantum efficiency of 90%, corresponding to responsivity $R = 0.6$ A/W at 850 nm. At the receiver, the antialiasing filter is a fifth-order Butterworth low-pass filter. For OFDM, we set the 3-dB cutoff frequency of the antialiasing filter equal to the first null of the OFDM spectrum [19]. For M -ary PAM (M -PAM), we set the 3-dB cutoff frequency to $0.8R_s$, where R_s is the symbol rate.

Typical high-performance FEC codes for optical systems have a threshold bit error ratio (BER) of the order of $P_b = 10^{-3}$. In order to provide a small margin, we compute the minimum required SNR to achieve $P_b = 10^{-4}$ for the different modulation formats. A BER $P_b = 10^{-4}$ corresponds to a gap of $\Gamma = 6.6$ dB. We choose a granularity $\beta = 0.25$ for the discrete bit-loading algorithms, since it is straightforward to design practical codes whose rates are multiples of 0.25.

We let R_s denote the symbol rate for unipolar M -PAM (in the special case of 2-PAM or OOK, $R_s = R_b$). We let R_s^{OFDM} denote the equivalent symbol rate for OFDM [19]. In an attempt to provide a fair comparison between unipolar M -PAM and OFDM, unless stated otherwise, we will let the two symbol rates be equal, $R_s^{\text{OFDM}} = R_s$. For all OFDM formats, we use an oversampling ratio of $M_s = 64/52 \approx 1.23$ to avoid noise aliasing. In this case, OFDM requires an analog-to-digital (A/D) converter sampling frequency of $M_s R_s^{\text{OFDM}}$. While an equalizer for M -PAM can employ an arbitrary rational sampling frequency such as $3/2$ to achieve good performance, an oversampling ratio of 2 is often chosen because it yields slightly better performance than $3/2$, while greatly simplifying the equalizer structure [19]. Assuming a bit rate $R_b = 10$ Gb/s and $R_s^{\text{OFDM}} = R_s$, the required A/D sampling frequency is 12.3 GHz for OFDM and 20 GHz for OOK.

Fig. 10 shows the receiver electrical SNR required to achieve a bit rate of 10 Gb/s for several fibers of 1-km length using ACO-OFDM and OOK. In order to make our results independent of the bit rate, we present our results in Fig. 10 as a function of the normalized delay spread D_T . The symbol rate is the same for both modulation schemes, i.e., $R_s^{\text{OFDM}} = R_s = 10$ GHz. For ACO-OFDM, the fast Fourier transform (FFT) size is $N = 1024$ and the number of used subcarriers is $N_u = 208$. We set the cyclic prefix equal to the duration (in samples) of the worst fiber impulse response, corresponding to $N_{\text{pre}} = 14$ samples measured at the OFDM symbol rate. For OOK, we use a fractionally spaced MMSE-DFE at an oversampling ratio of 2. We use the same number of taps for all fibers, which is chosen based on the worst fiber: 41 taps for the feedforward filter and 15 taps for the feedback filter.

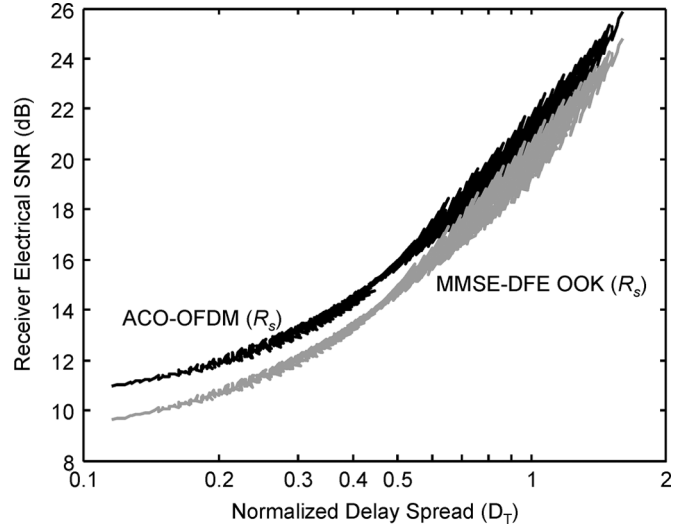


Fig. 10. Receiver electrical SNR required to obtain 10 Gb/s at $P_b = 10^{-4}$ for ACO-OFDM and OOK for fibers with 1-km length. The bit allocation granularity is $\beta = 0.25$ and ACO-OFDM has the same symbol rate as OOK ($R_s^{\text{OFDM}} = R_s = 10$ GHz).

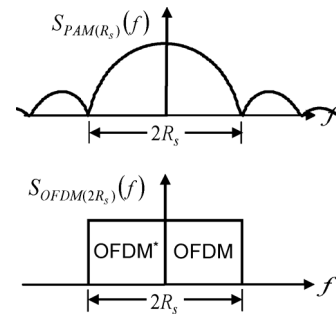


Fig. 11. Optical spectra of M -PAM and OFDM. The symbol rate for OFDM is twice that for M -PAM, $R_s^{\text{OFDM}} = 2R_s$.

In Fig. 10, we observe that ACO-OFDM requires a higher SNR than OOK for all fibers in our set when both modulations use the same symbol rate. In this case, which corresponds to a spectral efficiency of 1 bit/s/Hz, the performance difference is about 1 dB. ACO-OFDM requires a higher SNR than OOK because it requires an average of 4 bits (16-QAM) on the used subcarriers to compensate the information rate loss when half of the subcarriers are set to zero. However, we can improve the performance of OFDM by using more optical bandwidth (which also requires more electrical bandwidth). At a symbol rate (or baud rate) R_s , M -PAM requires an optical bandwidth of approximately $2R_s$, which corresponds to the interval between spectral nulls on either side of the carrier. On the other hand, OFDM requires a bandwidth of approximately R_s^{OFDM} [19]. Hence, for the same symbol rate as M -PAM ($R_s^{\text{OFDM}} = R_s$), OFDM requires half the bandwidth of M -PAM. If we double the symbol rate for OFDM, both modulations schemes use approximately the same optical bandwidth $2R_s$, as shown in Fig. 11.¹

¹The optical bandwidths stated here assume that the source linewidth is small compared to the modulation bandwidth. If the source linewidth is large, changing the symbol rate may have little effect on the optical bandwidth, although it does affect the electrical bandwidth.

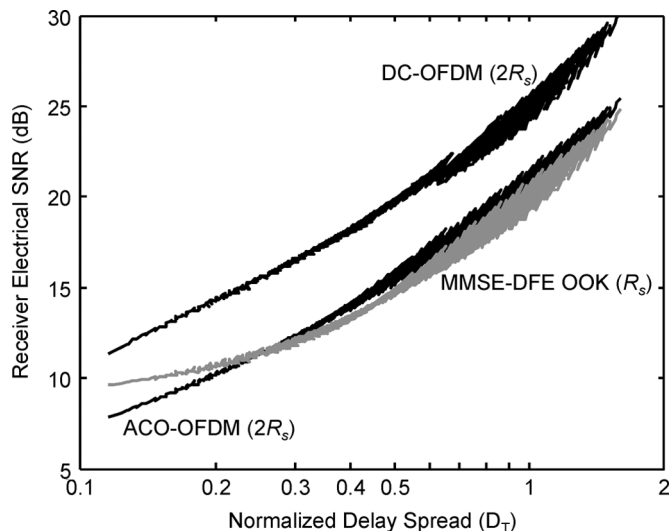


Fig. 12. Receiver electrical SNR required to achieve $P_b = 10^{-4}$ at 10 Gb/s for different modulations formats in fibers with 1-km length. The bit allocation granularity is $\beta = 0.25$. The symbol rate for all OFDM formats is twice that for OOK, $R_s^{\text{OFDM}} = 2R_s = 20$ GHz.

Fig. 12 shows the receiver electrical SNR required to achieve a bit rate of 10 Gb/s for several fibers of length 1 km when all the OFDM formats use twice the symbol rate of OOK, i.e., $R_s^{\text{OFDM}} = 2R_s = 20$ GHz. The sampling frequency required for OFDM in this case is $1.23 \times 20 = 24.6$ GHz. We set again the cyclic prefix equal to the duration of the worst fiber impulse response, obtaining $N_{\text{pre}} = 24$ samples measured at the OFDM symbol rate. The prefix penalty is computed as in [19]. We choose the number of used subcarriers N_u equal to 416 for DC-OFDM, such that the prefix penalty is negligible. The FFT size is $N = 1024$ for DC-OFDM. For ACO-OFDM, the FFT size is $N = 2048$, such that the number of used subcarriers is the same as DC-OFDM. For PAM-DMT, we set the FFT size to $N = 2048$ ($N_u = 832$), in order to make a fair comparison with ACO-OFDM.

In computing the optimized subcarrier power allocation for DC-OFDM, we cannot use (5) and (6) directly, since the clipping noise on each subcarrier depends on the power of all the subcarriers. Thus, we perform the power allocation iteratively. For a given power allocation, the SNR measured at each subcarrier is used to compute an updated water-filling solution. We repeat this process until the power allocation no longer changes. In addition to optimizing the power and bit allocation at each subcarrier, we need to optimize the dc bias for DC-OFDM. In order to minimize the dc bias, we use a bias level proportional to the square root of the electrical power. We define the proportionality constant as the bias ratio B_R , which is given by

$$B_R = \frac{\text{DC}_{\text{bias}}}{\sigma} \quad (25)$$

where $\sigma = \sqrt{P_{\text{elect}}}$ is the standard deviation of the electrical OFDM waveform. Using the B_R ensures that the water-filling solution minimizes the dc bias, and thus the optical power required. For example, in DC-OFDM, if the electrical power is excessively high, the dc bias will also be excessively high. A

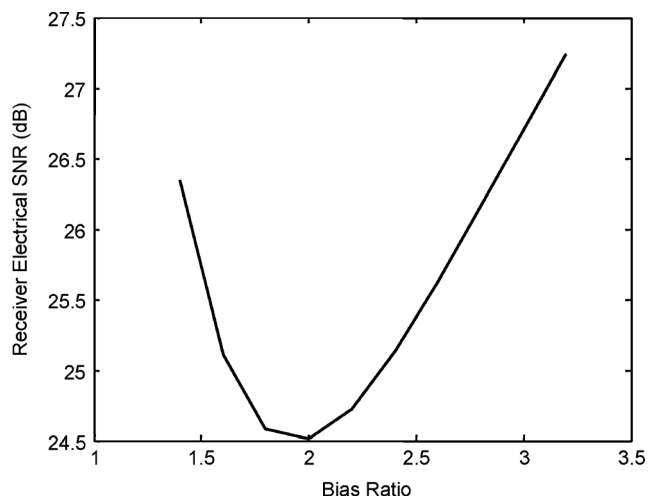


Fig. 13. Receiver electrical SNR required for DC-OFDM to achieve $P_b = 10^{-4}$ at 10 Gb/s for different values of the bias ratio in fiber 295.

high dc bias reduces the clipping noise, and therefore, the received SNR on each subcarrier is high. On the next iteration, the water-filling algorithm removes some of the excess electric power in order to lower the SNR to the desired value, and therefore the dc bias decreases. On the other hand, if the dc bias is too low, the clipping noise is excessively high, and therefore, the received SNR on each subcarrier is too low. On the next iteration, the water-filling algorithm adds more electrical power in order to increase the SNR to the desired value, and consequently the dc bias increases. The minimum required optical SNR is obtained by performing an exhaustive search on the B_R value, as shown in Fig. 13.

In Fig. 12, we observe again that OOK with MMSE-DFE requires the lowest SNR to achieve 10 Gb/s at $P_b = 10^{-4}$ for most fibers, even when all OFDM formats use twice the symbol rate of OOK. We note that when OFDM uses twice the symbol rate of OOK, OFDM is allowed to use twice the bandwidth it would normally require to transmit the same bit rate as OOK. Even with this advantage, all OFDM formats still perform worse than OOK for the majority of the fibers, as shown in Fig. 12. However, for fibers with a large bandwidth (>7 GHz), ACO-OFDM outperforms OOK. We note that in computing Fig. 12 for OOK with MMSE-DFE, we have used correct decisions at the input of the feedback filter. If we use detected symbols for the feedback filter input, the required SNR increases by 0.4 dB for fiber bandwidths less than 4 GHz, due to error propagation. For fiber bandwidths beyond 4 GHz, the increase in required SNR is less than 0.2 dB. The difference between ACO-OFDM and OOK is within 0.8 and 1 dB, so OOK with error propagation is still more power efficient than ACO-OFDM.

DC-OFDM requires the highest SNR because of the dc bias required to make the OFDM waveform nonnegative. Fig. 13 shows the receiver electrical SNR required for DC-OFDM for different B_R values. We can see that if the B_R is too high, then the required SNR is also high, because of the power wasted in the dc bias. On the other hand, if the B_R is too low, more power has to be allocated to each subcarrier to compensate for the high clipping noise, and therefore the required SNR increases.

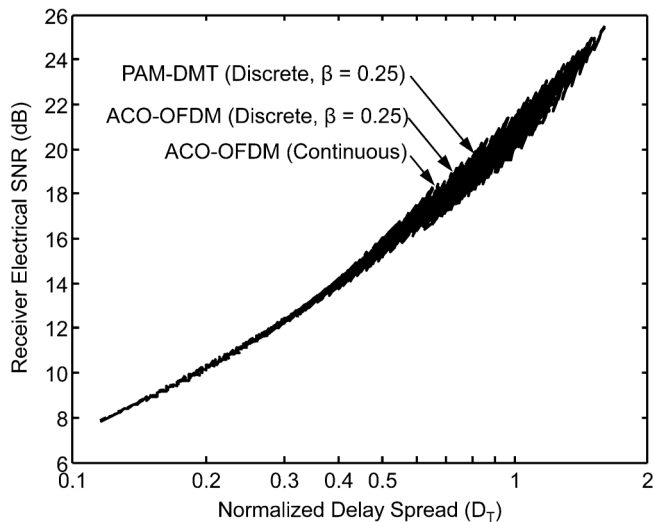


Fig. 14. Receiver electrical SNR required for various OFDM formats with continuous and discrete bit allocations to achieve $P_b = 10^{-4}$ at 10 Gb/s for fibers of 1-km length. The symbol rate for all OFDM formats is $R_s^{\text{OFDM}} = 20$ GHz.

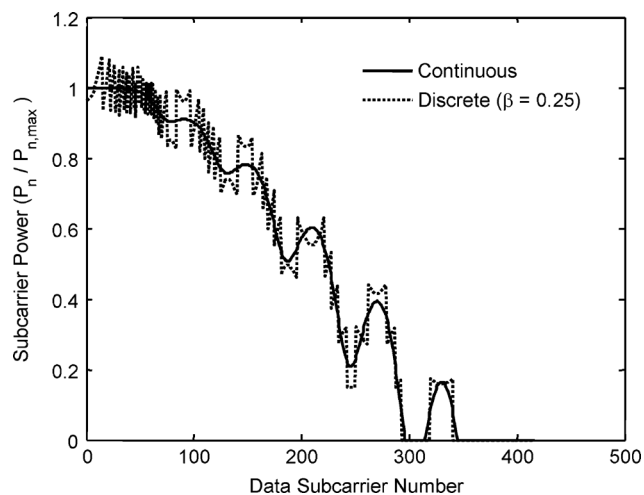


Fig. 15. Subcarrier power distribution for ACO-OFDM with continuous bit allocation and with discrete bit loading (with granularity $\beta = 0.25$) for 10 Gb/s at $P_b = 10^{-4}$ in fiber 10. The symbol rate is $R_s^{\text{OFDM}} = 20$ GHz.

Fig. 14 compares ACO-OFDM and PAM-DMT using $\beta = 0.25$ with ACO-OFDM using continuous bit allocation. In Fig. 14, we observe that there is no significant performance difference between PAM-DMT and ACO-OFDM. The difference in SNR between ACO-OFDM and PAM-DMT is less than 0.1 dB. This is to be expected, since for a high number of subcarriers, PAM-DMT converges asymptotically to the same performance as ACO-OFDM. Since PAM-DMT and ACO-OFDM have the same performance, we choose ACO-OFDM as the OFDM format for comparison for the remainder of the paper.

We also see that there is no significant difference between ACO-OFDM with discrete loading ($\beta = 0.25$) and ACO-OFDM with continuous bit allocation. This means that using OFDM with coding rates that are multiples of 0.25 is sufficient to achieve optimal power performance. The subcarrier power distribution for discrete and continuous ACO-OFDM is shown in Fig. 15.

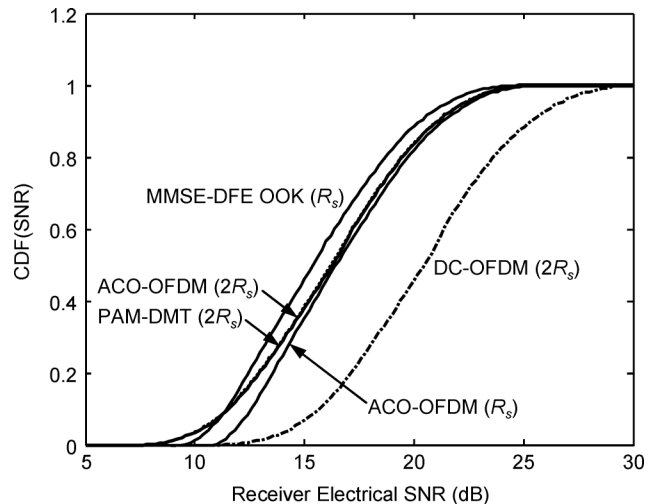


Fig. 16. CDF of the required receiver electrical SNR to obtain $P_b = 10^{-4}$ at 10 Gb/s for different modulation formats. The symbol rate for OOK is $R_s = 10$ GHz and the symbol rate for OFDM is the same or twice that for OOK, as indicated in the figure.

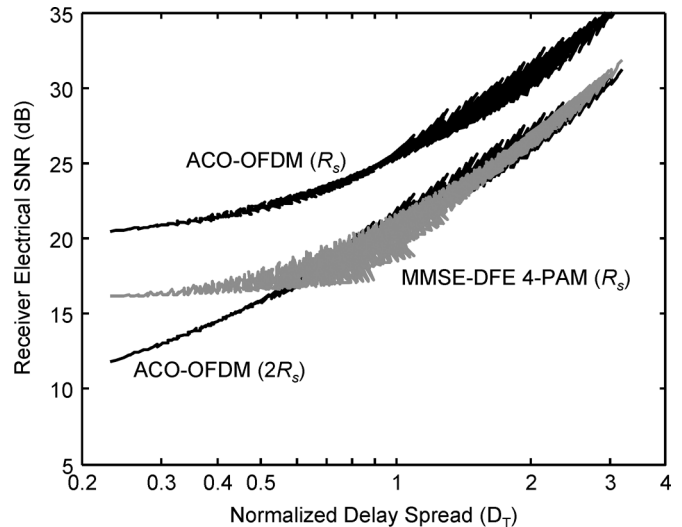


Fig. 17. Receiver electrical SNR required to obtain 20 Gb/s at $P_b = 10^{-4}$ for the different modulations formats for fibers of 1-km length. The bit allocation granularity is $\beta = 0.25$ and the symbol rate for 4-PAM is $R_s = 10$ GHz. The symbol rate for ACO-OFDM is the same or twice that for 4-PAM, as indicated in the figure.

Fig. 16 shows the cumulative distribution function (CDF) of the required SNR. In Fig. 16, we observe that OOK with MMSE-DFE requires less SNR for the majority of the fibers, as expected. Furthermore, we also notice that doubling the symbol rate for ACO-OFDM only improves the performance for fibers with low rms delay spreads. For high RMS delay spreads, doubling the symbol rate gives practically no performance increase.

It is also interesting to check if the same performance difference is obtained at higher spectral efficiencies, i.e., for unipolar M -PAM. Figs. 17 and 18 show the receiver electrical SNR required to achieve a bit rate of 20 Gb/s for ACO-OFDM and unipolar 4-PAM. The symbol rate for 4-PAM is kept constant at 10 GHz.

In Fig. 17, we observe that 4-PAM requires the lowest SNR to achieve 20 Gb/s at $P_b = 10^{-4}$ for most fibers. This can also

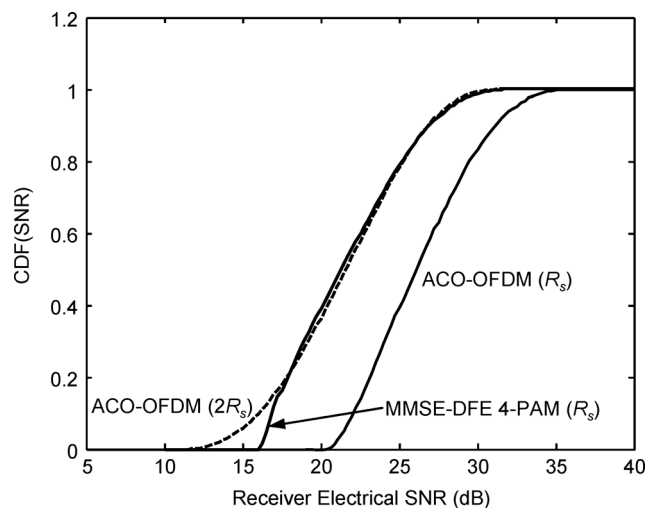


Fig. 18. CDF of the required receiver electrical SNR to obtain 20 Gb/s at $P_b = 10^{-4}$ for different modulation formats. The symbol rate for 4-PAM is $R_s = 10$ GHz and the symbol rate for ACO-OFDM is the same or twice that for 4-PAM, as indicated in the figure.

be easily seen in Fig. 18. We observe that the difference in SNR between ACO-OFDM and unipolar 4-PAM is about 4 dB when both modulations use the same symbol rate. We conclude that increasing the spectral efficiency from 1 bit/s/Hz (see Fig. 10) to 2 bit/s/Hz (Fig. 17) increases difference in SNR requirement between ACO-OFDM and M -PAM from 1 to 4 dB. This is to be expected, since increasing the spectral efficiency from 1 bit/s/Hz to 2 bit/s/Hz for ACO-OFDM requires doubling the average number of bits on each subcarrier from 4 bits (16-QAM) to 8 bits (256-QAM) when the symbol rate for ACO-OFDM is the same as that for M -PAM.

We also observe that ACO-OFDM with twice the symbol rate of 4-PAM has practically the same performance as 4-PAM. Furthermore, ACO-OFDM now outperforms M -PAM for a larger fraction of fibers. However, this performance increase for ACO-OFDM requires doubling the electrical bandwidth and increasing the sampling frequency from 12.3 to 24.6 GHz, which is 23% higher than the sampling frequency required for 4-PAM using an oversampling ratio of two, i.e., 20 GHz.

VI. CONCLUSION

We have evaluated the performance of three different OFDM formats in IM/direct-detection optical systems for multimode fibers: DC-OFDM, ACO-OFDM, and PAM-DMT. We have derived the optimal power allocation for PAM-DMT and have shown that the performance of PAM-DMT converges asymptotically to that of ACO-OFDM as the number of subcarriers increases. We have also shown how to minimize the average optical power required for DC-OFDM to achieve a specified error probability by iteratively adjusting the subcarrier power allocation and the bias ratio. For a given symbol rate, we have found that unipolar M -PAM with MMSE-DFE has a better optical power performance than all OFDM formats. Furthermore, we have found that the performance difference between M -PAM and OFDM increases as the spectral efficiency increases. We have shown that at a spectral efficiency of 1 bit/s/Hz, OOK performs better than ACO-OFDM with twice the symbol rate of

OOK. For higher spectral efficiencies, ACO-OFDM at twice the symbol rate of M -PAM performs close to M -PAM, but requires more electrical bandwidth and 23% faster A/D converters than those required for M -PAM at 2 samples per symbol.

ACKNOWLEDGMENT

The authors would like to thank M. Shemirani for helpful discussions and suggestions.

REFERENCES

- [1] J. M. Tang, P. M. Lane, and K. A. Shore, "Transmission performance of adaptively modulated optical OFDM signals in multimode fiber links," *IEEE Photon. Technol. Lett.*, vol. 18, no. 1, pp. 205–207, Jan. 2006.
- [2] S. Randel, F. Breyer, and S. C. J. Lee, "High-speed transmission over multimode optical fibers," presented at the presented at the Opt. Fiber Commun. Conf./Collocated Natl. Fiber Opt. Eng. Conf., San Diego, CA, 2008, Paper OWR2.
- [3] J. M. Tang, P. M. Lane, and K. A. Shore, "High-speed transmission of adaptively modulated optical OFDM signals over multimode fibers using directly modulated DFBs," *J. Lightw. Technol.*, vol. 24, no. 1, pp. 429–441, Jan. 2006.
- [4] J. Armstrong, B. J. C. Schmidt, D. Kalra, H. A. Suraweera, and A. J. Lowery, "Performance of asymmetrically clipped optical OFDM in AWGN for an intensity modulated direct detection system," in *Proc. IEEE Global Commun. Conf.*, 2006, pp. 1–5.
- [5] S. C. J. Lee, S. Randel, F. Breyer, and A. M. J. Koonen, "PAM-DMT for intensity-modulated and direct-detection optical communication systems," *IEEE Photon. Technol. Lett.*, vol. 21, no. 23, pp. 1749–1751, Dec. 2009.
- [6] X. Q. Jin, J. M. Tang, P. S. Spencer, and K. A. Shore, "Optimization of adaptively modulated optical OFDM modems for multimode fiber-based local area networks," *J. Opt. Netw.*, vol. 7, no. 3, pp. 198–214, 2008.
- [7] S. C. J. Lee, F. Breyer, S. Randel, H. P. A. van den Boom, and A. M. J. Koonen, "High-speed transmission over multimode fiber using discrete multitone modulation," *J. Opt. Netw.*, vol. 7, no. 2, pp. 183–196, 2008.
- [8] M. B. Shemirani and J. M. Kahn, "Higher-order modal dispersion in graded-index multimode fiber," *J. Lightw. Technol.*, vol. 27, no. 23, pp. 5461–5468, Dec. 2009.
- [9] J. Campello, "Optimal discrete bit loading for multicarrier modulation systems," presented at the presented at the IEEE Symp. Info. Theory, Cambridge, MA, 1998.
- [10] G. D. Forney and G. Ungerboeck, "Modulation and coding for linear Gaussian channels," *IEEE Trans. Info. Theory*, vol. 44, no. 6, pp. 2384–2415, Oct. 1998.
- [11] J. M. Cioffi, G. P. Dudevoir, M. V. Eyuboglu, and G. D. Forney, Jr, "MMSE decision-feedback equalizers and coding—Part II: Coding results," *IEEE Trans. Commun.*, vol. 43, no. 10, pp. 2595–2604, Oct. 1995.
- [12] W. Yu, G. Ginis, and J. M. Cioffi, "An adaptive multiuser power control algorithm for VDSL," in *Proc. IEEE Global Commun. Conf.*, 2001, vol. 1, pp. 394–398.
- [13] P. Pepeljugoski, S. E. Golowich, A. J. Ritger, P. Kolesar, and A. Risteski, "Modeling and simulation of next-generation multimode fiber links," *J. Lightw. Technol.*, vol. 21, no. 5, pp. 1242–1255, May 2003.
- [14] P. Pepeljugoski, M. J. Hackert, J. S. Abbott, S. E. Swanson, S. E. Golowich, A. J. Ritger, P. Kolesar, Y. C. Chen, and P. Pleunis, "Development of system specification for laser-optimized 50- μ m multimode fiber for multigigabit short-wavelength LANs," *J. Lightw. Technol.*, vol. 21, no. 5, pp. 1256–1275, May 2003.
- [15] X. Q. Jin, J. M. Tang, K. Qiu, and P. S. Spencer, "Statistical investigations of the transmission performance of adaptively modulated optical OFDM signals in multimode fiber links," *J. Lightw. Technol.*, vol. 26, no. 18, pp. 3216–3224, Sep. 2008.
- [16] X. Zheng, J. M. Tang, and P. S. Spencer, "Transmission performance of adaptively modulated optical OFDM modems using subcarrier modulation over worst-case multimode fiber links," *IEEE Commun. Lett.*, vol. 12, no. 10, pp. 788–790, Oct. 2008.
- [17] J. M. Kahn and J. R. Barry, "Wireless infrared communications," *Proc. IEEE*, vol. 85, no. 2, pp. 265–298, Feb. 1997.
- [18] J. B. Carruthers and J. M. Kahn, "Modeling of nondirected wireless infrared channels," *IEEE Trans. Commun.*, vol. 45, no. 10, pp. 1260–1268, Oct. 1997.
- [19] D. J. F. Barros and J. M. Kahn, "Optimized dispersion compensation using orthogonal frequency-division multiplexing," *J. Lightw. Technol.*, vol. 26, no. 16, pp. 2889–2898, Aug. 2008.

Daniel J. F. Barros received the “*Licenciatura*” degree (Hons.) in electrical and electronics engineering from the University of Porto, Portugal, in 2004, and the M.S. degree in electrical engineering from Stanford University, Stanford, CA, in 2007, where he is currently working toward the Ph.D. degree in electrical engineering.

His research interests include single-mode optical-fiber communication, digital signal processing, and RF circuits.

Joseph M. Kahn (M’90–SM’98–F’00) received the A.B., M.A., and Ph.D. degrees in physics from University of California, Berkeley, (UC Berkeley) in 1981, 1983, and 1986, respectively.

From 1987 to 1990, he was at AT&T Bell Laboratories, Crawford Hill Laboratory, Holmdel, NJ. He demonstrated multi-Gb/s coherent optical fiber transmission systems, setting world records for receiver sensitivity. From 1990 to

2003, he was on the faculty of the Department of Electrical Engineering and Computer Sciences, UC Berkeley, performing research on optical and wireless communications. Since 2003, he has been a Professor of electrical engineering at Stanford University, Stanford, CA, where he heads the Optical Communications Group. In 2000, he helped found StrataLight Communications (now Opnext Subsystems), where he served as the Chief Scientist from 2000 to 2003. His current research interests include rate-adaptive and spectrally efficient modulation and coding methods, coherent detection and associated digital signal processing algorithms, digital compensation of fiber nonlinearity, high-speed transmission in multimode fiber, and free-space systems.

Dr. Kahn received the National Science Foundation Presidential Young Investigator Award in 1991. During 1993–2000, he served as a Technical Editor of IEEE PERSONAL COMMUNICATIONS MAGAZINE. Since 2009, he has been an Associate Editor of IEEE/OSA JOURNAL OF OPTICAL COMMUNICATIONS AND NETWORKING.